DRIFTWAVE-BASED MODELING OF POLOIDAL SPIN-UP PRECURSOR AND STEP-WISE EXPANSION OF TRANSPORT BARRIERS

by

G.M. STAEBLER, J.E. KINSEY, P. ZHU, G. BATEMAN, W. HORTON, A.H. KRITZ, T. ONJUN, A. PANKIN, and R.E. WALTZ

DECEMBER 2000

DISCLAIMER

DRIFTWAVE-BASED MODELING OF POLOIDAL SPIN-UP PRECURSOR AND STEP-WISE EXPANSION OF TRANSPORT BARRIERS

by

G.M. STAEBLER, J.E. KINSEY,[†] P. ZHU,[‡] G. BATEMAN,[†] W. HORTON,[‡]
A.H. KRITZ,[†] T. ONJUN,[†] A. PANKIN,[†] and R.E. WALTZ

[†]Lehigh University
[‡]Institute for Fusion Studies, The University of Texas

DriftWave-Based Modeling of Poloidal Spin-up Precursor and Step-wise Expansion of Transport Barriers

G.M. Staebler,[1] J.E. Kinsey,[2]* P. Zhu,[3] G. Bateman,[2] W. Horton,[3] A.H. Kritz,[2] T. Onjun,[2] A. Pankin,[2] and R.E. Waltz[1]

[1]General Atomics, P.O. Box 85608, San Diego, California 92186-5608
[2]Lehigh University, Bethlehem, Pennsylvania 18015
[3]Institute for Fusion Studies, The University of Texas at Austin, Austin Texas 78712
*Present address: General Atomics

Abstract. The rich phenomenology of internal transport barriers observed in tokamaks includes a poloidal spin-up precursor for balanced injection neutral beam heating and step-wise expansion of the barrier for unbalanced injection. Examples of numerical simulations of these phenomena are presented. Two driftwave-based predictive transport models (GLF23 and Multi-Mode) are used. Both models include the suppression of ion temperature gradient modes as the E×B shear approaches the computed maximum linear growth rate. Modeling of discharges with internal transport barriers from the DIII–D, JET and TFTR tokamaks are compared.

The suppression of ion temperature gradient (ITG) mode turbulence by equilibrium E×B velocity shear has been demonstrated in 3D numerical simulations [1]. The simulations were shown to approximately follow a simple "quench rule." The turbulence is quenched (completely suppressed) when the E×B shear rate ($\gamma_{E \times B}$) exceeds the maximum linear ITG mode growth rate of the wavenumber spectrum (γ_{ITG}) computed without E×B shear. The quench rule is implemented in the models by introducing a net growth rate $\gamma_{net} = \gamma_{ITG} - \alpha_{E \times B} \gamma_{E \times B}$ which is set to zero when it is negative. This mechanism has been shown to be consistent with enhanced confinement regimes in tokamaks ranging from H–mode to VH–mode to internal transport barriers [2]. Using simple models incorporating the quench rule, much of the phenomenology of E×B shear suppression of transport has been explored giving useful insight into experiments and leading to new methods of controlling transport [3]. In order to have a predictive transport model incorporating the quench rule, the maximum linear ITG mode growth rate must be computed. Only then can the dependence of the transport suppression threshold on the safety factor profile, the Shafranov shift and many other important factors be accurately modeled.

Here we report on some of the recent success of driftwave-based transport modeling of internal transport barriers (ITB). The term driftwave-based is used in this paper to mean a theoretical model which computes the linear growth rates of drift-waves locally and then computes the transport due to these modes using quasilinear theory and a model for the saturated fluctuation amplitude. The two specific models which fit this description are the Multi-Mode model (MMM95) which pioneered this methodology [4–6] using the Wieland-Nordman fluid model [7–9] and the GLF23 model [10] which adopted the same method but uses a gyro-Landau fluid [11] treatment of the driftwaves including Landau damping and other kinetic effects rather than the fluid limit employed by the Weiland-Nordman model. Both models include the ITG mode and trapped electron modes and use the quench rule to include E×B velocity shear. This goes beyond established theory since the non-linear simulations [1] were only for ITG modes with no trapped electrons. However, it is known from linear theory that trapped electron modes can be stabilized by E×B shear [12]. The GLF23 model has electron temperature gradient (ETG) modes contributing to electron thermal transport. These modes are not subject to the quench rule due to their large growth rates. The Multi-Mode model has a formula for kinetic ballooning modes which gives additional transport in all channels (heat, particle) and is also not affected by E×B shear. Thus, the transport in the ITB region where ITG/TEM modes are quench has quite different physics in the two models.

Three examples are given in the paper illustrating the ability of the models to predict the onset and development of internal transport barriers in tokamaks. The first example is a Multi-Mode simulation of the evolution of an optimized shear discharge on the JET tokamak [13]. In this case the temperatures, density, q-profile, sources, sinks and neutrals were evolved with Multi-

Mode but the toroidal rotation was taken from the experimental data. The second case is a GLF23 simulation of a DIII–D discharge [14]. Here the toroidal rotation was evolved but not the density or q-profile. The sources and sinks were taken from ONETWO analysis. The step-wise expansion of the transport barrier is shown to result from a competition of the toroidal rotation and diamagnetic plus poloidal velocity contributions to the E×B velocity. The third case is a modified GLF23 simulation of a TFTR discharge. In this discharge a poloidal spin-up precursor to the internal transport barrier was observed [15]. This is reproduced by the model evolving the ion temperature and E×B velocity in a very high resolution computation with a special numerical method [16]. It is worth noting that the driftwave-based models pose difficult numerical challenges. The quasilinear theory produces a flux (energy, particles, viscous stress). The transport coefficients (diffusivity, convection velocity) can be defined in different ways from these fluxes. The fluxes are strongly non-linear functions of the profile gradients with cross couplings (off-diagonal terms) of similar strength to the diagonal terms. The Multi-Mode model example was run on the BALDUR transport code [17]. The two GLF23 examples were run on the XPTOR code [18]. All three cases used different methods for defining the transport coefficients from the fluxes.

Before discussing the three cases, a brief comment on the determination of the E×B velocity is needed. The neoclassical equations for the transport of momentum are usually given in terms of the toroidal (φ) and parallel ($\|$) momentum balance equations [19] ($< >$ = flux surface average).

$$\frac{\partial}{\partial t}(m_i n_i u_\varphi) + \left\langle (\overline{\nabla} \bullet \overline{\overline{\Pi}}^A - \overline{S}) \bullet \hat{e}_\varphi \frac{R}{R_0} \right\rangle = 0 \quad , \tag{1}$$

where

$$u_\varphi = \left\langle \overline{V} \bullet \hat{e}_\varphi R \right\rangle / R_0 \quad , \tag{2}$$

$$\frac{\partial}{\partial t}(m_i n_i u_\|) + \left\langle \left[\overline{\nabla} \bullet \left(\overline{\overline{\Pi}}^{neo} + \overline{\overline{\Pi}}^A \right) - \overline{S} \right] \bullet \frac{\overline{B}}{B_0} \right\rangle = 0 \quad , \tag{3}$$

where

$$u_\| = \left\langle \overline{V} \bullet \overline{B} \right\rangle / B_0 \quad . \tag{4}$$

Here Π^{neo} is the collisional contribution to the viscous stress which vanishes in the toroidal direction, (φ), and Π^A is the viscous stress due to turbulence [12]. The external momentum source vector is $\overline{S}$. The magnetic field B_0 and major radius R_0 are evaluated at the magnetic axis. The inertia terms have been neglected as small. The neoclassical parallel viscous stress

$$\left\langle \overline{\nabla} \bullet \overline{\overline{\Pi}}^{neo} \bullet \frac{\overline{B}}{B_0} \right\rangle = \mu^{neo} \left(u_\theta - K \frac{\partial T}{\partial \rho} \right) \quad . \tag{5}$$

is usually assumed to be much larger than the contribution from turbulence [19], The parallel momentum balance is also assumed to come to equilibrium faster than the other transport equations. With these orderings, the poloidal velocity $u_\theta = \rho B_0 \left\langle V_\theta / B_\theta \right\rangle / (R_0 q)$ is determined by setting the neoclassical parallel viscous stress [Eq. (5)] to zero. This ordering has also been used in the first two examples of this paper. The E×B velocity $u_{E\times B} = c/B_0(d\Phi/d\rho)$ is determined from radial force balance to be

$$u_{E \times B} + \frac{c}{eB_0 n_i} \frac{dp_i}{d\rho} = \left(c_2 u_\theta - \frac{\rho}{R_0 q} u_\varphi \right) \Big/ c_3 \quad , \tag{6}$$

where

$$c_1 = \frac{\langle B^2 \rangle}{B_0^2}, \; c_2 = \frac{\langle RB_\varphi \rangle}{R_0 B_0}, \; c_3 = \frac{\langle R^2 \rangle}{R_0^2} \quad , \tag{7}$$

Using the neoclassical solution for the poloidal velocity, the E×B velocity is eliminated using Eq. (6) in terms of the three fields (u_φ, p_i, n_i) which are evolved by the transport equations. One problem with this approach is that the quasilinear fluxes become functions of the second derivatives of the ion temperature and density through the E×B shear. This makes the transport equations third order in the gradients, introducing the need for unphysical boundary conditions [20]. If the ordering assumptions are relaxed so that the parallel momentum balance equation is on the same footing as the others, then an equation for the time evolution of the E×B velocity can be obtained [16]. The radial force balance equation [Eq. (6)] is used to eliminate the poloidal velocity in favor of the E×B velocity. The toroidal and parallel momentum balance equations are then combined to get an equation with just the toroidal and E×B velocities using

$$\frac{\rho}{R_0 q} \frac{\left(c_1 u_\varphi - c_2 u_\parallel \right)}{\left(c_2^2 - c_1 c_3 \right)} = u_{E \times B} + \frac{c}{eB_0 n_i} \frac{dp_i}{d\rho} \quad , \tag{8}$$

The resulting equation is

$$\frac{\partial}{\partial t} \left[m_i n_i \left(u_{E \times B} + \frac{c}{eB_0 n_i} \frac{dp_i}{d\rho} \right) \right] + \left\langle \left[\overline{\nabla} \bullet \left(\overline{\overline{\Pi}}^A + \overline{\overline{\Pi}}^{neo} \right) - \overline{S} \right] \bullet \hat{e}_{E \times B} \right\rangle = 0 \quad , \tag{9}$$

where

$$\hat{e}_{E \times B} = \frac{\rho}{R_0 q} \left[c_1 \frac{RB_\varphi}{R_0 B_0} \hat{e}_\varphi - c_2 \frac{\overline{B}}{B_0} \right] \Big/ \left(c_2^2 - c_1 c_3 \right) \quad . \tag{10}$$

Using Eq. (9) keeps all of the turbulent fluxes (and viscous stresses) first order in the derivative of the time dependent fields ($n_i, p_e, p_i, u_\varphi, u_{E \times B}$). This equation was used only in the third example of this paper. It is required to model the strong deviation from neoclassical poloidal flow observed in the poloidal spin-up precursor.

2. Multi-Mode Model Simulations

The Multi-Mode transport model is used in the BALDUR time-dependent predictive transport modeling code to simulate the onset and time evolution of internal transport barriers in high performance JET and DIII–D discharges [13]. These transport simulations compute radial profiles as a function of time for the electron and ion temperature, hydrogenic and impurity ion densities, magnetic q-value, sources and sinks of heat and particles, and neutral particle densities. Boundary conditions are taken from experimental data just inside the separatrix or at the top of the H–mode pedestal, when that pedestal forms. The toroidal velocity profile as a function of time is taken from experimental measurements, while the poloidal velocity profile is computed from neoclassical theory [21].

The JET discharges are particularly complex: The BALDUR simulations follow the transition from Ohmic to L–mode, to the formation of an internal transport barrier, to the transition to H–mode (implemented as a time-dependent boundary condition in our simulations), and then to the subsequent motion of the internal transport barrier. The plasma current is ramped up while radio frequency and neutral beam injection pre-heating is used to produce a broad current profile with low magnetic shear over a broad central region of the plasma.

The time evolution of the ion temperature profile for JET discharge 40542 is shown in Fig. 1, with results from the simulation shown in the left panel and corresponding experimental measurements shown in the right panel. The curves in this figure show the ion temperature at equally spaced intervals in normalized minor radius as a function of time. The top curve in this figure represents the peak temperature as a function of time, which is generally at or near the magnetic axis, while the bottom curve represents the lowest temperature, which is generally at the edge of the plasma. Internal transport barriers are characterized by wider spacing between adjacent curves (steeper gradients). It can be seen in Fig. 1 that an internal transport barrier forms near the magnetic axis (close to top curve) between 45.8 and 46.5 s in both the simulation (left panel) and the experiment (right panel). The transport barrier then moves closer to the edge of the plasma (lower curves) between 46.5 and 46.9 s in both simulation and experiment. Similar behavior is observed in simulations of other high-performance discharges in JET and DIII–D [21].

The simulation shown here uses a recent version of the Multi-Mode model with E×B flow shear stabilization using the quench rule in a Weiland model for drift modes that includes finite beta and low magnetic shear effects, as well as a Bateman-Scott model for drift Alfvén modes near the plasma edge [6]. Similar results are obtained using the Hamaguchi-Horton stabilization model that includes the effects of low magnetic shear and high flow shear [22]. In this Hamaguchi-Horton model, the quasi-linear transport coefficients are divided by $1+(\gamma_s/\gamma_{sc})^2$, where $\gamma_{sc} \approx 1$ and

$$\gamma_s = \sqrt{\frac{m_i}{T_e}} \left| \frac{R \partial_\psi (E_r/RB_\theta)}{\partial_\psi \ln q} \right| \quad . \tag{11}$$

This model enhances the ExB shear suppression in regions of weak magnetic shear. Note that the turbulence is reduced but not quenched in the Hamaguchi-Horton model. In this simulation, each of the three contributions to the E×B velocity [Eq. (6)] have comparable magnitude during the formation and motion of the internal transport barrier. The flow shear in the poloidal velocity (U_θ) contribution has a sharp positive peak at the inner edge of the transport barrier and a negative peak at the outer edge (as a function of minor radius). The peak value of flow shear in the toroidal velocity (U_φ) contribution (taken from experimental measurements in this simulation) remains at the outer edge of the internal transport barrier as
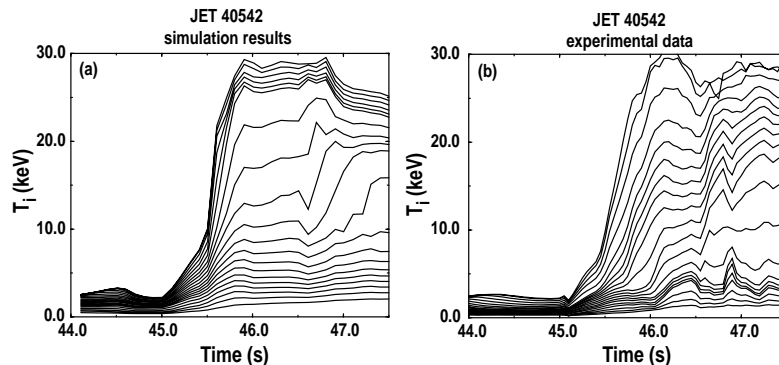

FIG. 1. *Ion temperature as function of time at equally spaced intervals in normalized minor radius in simulation (left) and experiment (right) for JET discharge 40542 with major radius 2.9 m, minor radius 0.94 m, toroidal field 3.6 T, plasma current 3.3 MA, line averaged density $2.5 \times 10^{19}/m^3$, and 17 MW NBI heating. From Ref. 13.*

the barrier shifts outward in minor radius between 46.0 and 47.5 s. The timing and location of the ITB transition is sensitive to the multiplier $\alpha_{E \times B}$ in the quench rule. This multiplier is known to vary with magnetic shear and elongation from the non-linear simulations but is taken to be a constant in the models. It has not been possible to obtain a good fit to a variety of discharges with a single value of $\alpha_{E \times B}$. More non-linear simulations are needed to develop a model for the parametric dependencies in $\alpha_{E \times B}$. The ITB threshold is a critical test of the E×B shear suppression model and its dependence on local plasma conditions.

3. GLF23 Simulation of Step-Wise Barrier Expansion

The GLF23 transport model has been used to dynamically follow E×B shear driven bifurcations in the energy and toroidal momentum confinement in DIII–D discharges with an internal transport barrier [14].Taking the density profiles, equilibrium, sources, and sinks from ONETWO analysis, the simulations are initialized with temperature and toroidal velocity profiles scaled down from the experimental profiles (at a given diagnostic time) to pre-barrier levels and the temperature and toroidal velocity profiles are evolved while self-consistently computing the effects of E×B shear stabilization using the model predicted profiles. The ITB is predicted to form and expand in a step-wise fashion with the core temperatures and toroidal rotation displaying an abrupt series of jumps during the barrier formation and expansion. These results are consistent with experimental observations.

In Fig. 2, the dynamic formation of an ITB resulting from an E×B shear driven bifurcation is demonstrated for a DIII–D negative central shear (NCS) discharge with an L–mode edge. Shown are the ion temperature and toroidal velocity predicted by the GLF23 model versus time. In the simulations, the step-transitions are a direct result of local E×B driven transport bifurcations. At each transition, dips in the electron temperatures and toroidal velocity are clearly evident as the E×B shear rate drops below the maximum linear growth rate at the leading edge of the barrier. As a result, E×B shear stabilization is transiently lost and the local thermal and toroidal momentum transport increases dramatically. The stiffness of the model then results in rapid propagation of the perturbation across the plasma core. Here, the dips are due to competition between the toroidal and diamagnetic plus poloidal velocity terms within the E×B shear rate which frustrates the otherwise continuous expansion of the ITB. The shear in the diamagnetic plus poloidal terms has the opposite sign from the toroidal rotation shear at the leading edge of the barrier. Since the toroidal rotation term dominates, a local increase in the ion temperature gradient reduces the net E×B shear at the front of the barrier which can cause a transient loss of E×B shear suppression. A smooth ITB expansion is predicted for counter NBI since the sign of the toroidal rotation shear is now the same as the diamagnetic + poloidal velocity shear. Steps have not been observed in counter-injected DIII–D discharges with ITB's. The barrier expansion phase begins deep in the core region where the underlying drift-wave transport is stabilized by negative magnetic shear, high T_i/T_e, and fast ion dilution, and the toroidal rotation dominates the E×B shear. The ITB expands through a series of step-transitions until the positive magnetic shear region is reached and the E×B velocity shear can no longer exceed the rising ITG growth rate.
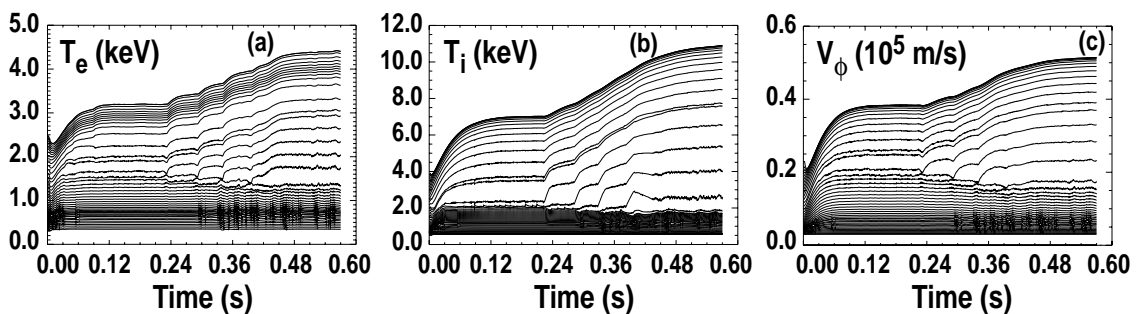

FIG. 2. *Time evolution of electron and ion tempertures and toroidal velocity predicted by the GLF23 model for DIII–D NCS discharge 87436. Values are shown at various radii with spacing of $\Delta\rho=0.02$. From Ref. 14.*

Overall, we find that both the height and the timing of the steps accompanying the expansion of the barrier front is sensitive to the proximity to the E×B shear driven ITB threshold and the rate in which it is approached. The ITB threshold is determined by the plasma conditions including, for example, density and temperature gradients, auxiliary heating power, and toroidal momentum input. Time variations in the densities, q-profile, sources, and sinks all impact the character, timing, and number of transitions (if present) by changing the underlying transport and E×B shear profile. Here, those quantities were held fixed in time and therefore we do not attempt a quantitative comparison of the timing of the steps with experimental data. There are other mechanisms which could cause step-wise expansions in the experiments, like MHD instabilities slowing the expansion across low order rational safety factor surfaces. The modeling shows that the drift-wave physics can also produce step-wise expansion dynamics.

4. Simulation of a Poloidal Spin-Up Precursor

The third example is a simulation of a TFTR discharge [15]. This discharge had reversed magnetic shear near the center and made a transition to enhanced confinement after the neutral beam power was increased. The neutral beam power was balanced for no net toroidal torque. Before the strong rise in stored energy indicating the formation of an internal transport barrier, a remarkably large poloidal velocity was observed to develop in a very narrow layer as shown in Fig. 3(a). This is the poloidal velocity of carbon but the velocity is so large compared to the diamagnetic velocity that it is by far the dominant contribution to the E×B velocity. This poloidal spin-up precursor grows up to its peak within the 20 ms integration time of the measurement. It then decays away over some 100 ms.

An analytic model has been used to show that this monopolar velocity excursion can be fit by a solution to the momentum balance equations [Eq. (2) and (5)] called a jet solution [23]. The poloidal flow is generated by an instability of the equations. When the E×B velocity shear is in the range where the magnitude of the turbulent viscous stress is dropping with increasing velocity shear, due to the reduction of the driftwave turbulence, the incremental viscosity (minus the derivative of the viscous stress with respect to the E×B velocity shear) is negative. A negative incremental viscosity produces an instability in the poloidal velocity with a growth rate that increases with the wavenumber of the perturbation squared [16]. Due to the presence of the neoclassical viscous damping of the poloidal velocity, this instability saturates at a wavenumber determined by the ratio of the collisional damping rate to the incremental viscosity due to turbulence. A narrow monopolar E×B velocity excursion from its neoclassical value is the quasi-steady state on the collisional damping rate time scale. This steady state jet solution was shown to be a type of topological soliton [23]. The integral of the velocity excursion is topologically conserved.

In Fig. 3(b) is shown a numerical solution of a modified version of the GLF23 model [16] for the same TFTR discharge at 1.824 s. Only the ion temperature and E×B velocity were evolved. The electron temperature profile was taken from the experiment. It does not participate directly in the determination of the E×B velocity. The sources and densities, electron temperature, toroidal velocity , magnetic geometry etc. were interpolated in time from the TRANSP analysis of TFTR discharge 104981. The simulation was run from 1.79–1.85 s. A complete discussion of the simulation in Fig. 3(b) and the special numerical scheme used will be reported in Ref. 16. The toroidal velocity from the experiment was used but it does not contribute to the narrow jet. A very fine grid was used (300 grid points over the full radius). The time step was (0.12 ms), which is shorter than the poloidal damping time (3.9 ms) at the radius of the jet. The E×B velocity jet grew up spontaneously in a few milliseconds close to the same location as observed in the experiment. The growth rate begins to increase rapidly with radius at this location. The jet solution persists for about 40 ms before decaying as the experimental profiles evolve. The ion temperature shows some steepening at the location of the jet. However, since the ion neoclassical thermal diffusion is much larger than the collisional gyroviscosity [24] the change in the E×B velocity gradient is much larger than the change in the temperature gradient. The analytic model [23] showed that the jet
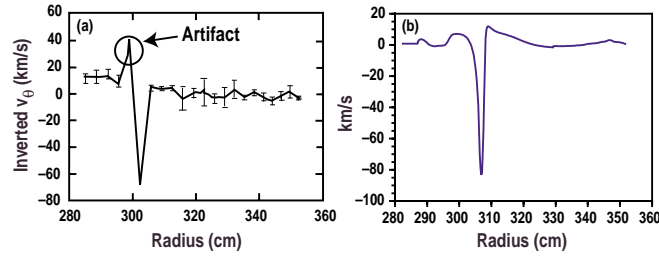
FIG. 3. Poloidal velocity of c^{+6} ions (a) measure for TFTR discharge 104981 at 1.81 s (Fig. 2 of Ref. 15). The E$\times$B velocity (b) computed with GLF23 at 1.824 s modeling the same TFTR discharge.

solution shrinks and then disappears as the diamagnetic velocity gradient builds. Once the diamagnetic velocity gradient is large enough to quench the turbulence no jet can exist.

The numerical simulation shows that the jet is somewhat fluctuating with finer scale features coming and going. These finer scale fluctuations are partially suppressed in the numerical scheme for numerical stability so the jet shown in Fig. 3(b), which spans about 12 grid points, is in effect averaged over the grid-scale and the time step. The measurement of the poloidal spin-up precursor is primarily on just one channel and is averaged over 20 ms. The spatial resolution is 3 cm [15]. It may be that the poloidal velocity is not steady but is bursty on finer time scales than the 20 ms integration time. The numerical simulation tends to have this property with the bursts appearing in the same localized region.

The agreement between the simulation and the experiment in this case is only achieved by adjusting the GLF23 model parameters. This departs from the philosophy of the model since it has been constructed by fitting to theoretical calculations (growth rates and saturated fluctuations level) without adjustment from experimental data [10]. In order to get a good fit to the ion temperature profile the fast ion and impurity dilution had to be eliminated. The trapped electron mode was giving a large ion energy pinch due to the hollow thermal ion density. The multiplier ($\alpha_{E\times B}$) on the E$\times$B shear also had to be turned down significantly. The ion temperature profile was well fit with no E$\times$B shear term. The Shafranov shift was sufficient to improve ion transport. This is consistent with the fact that the experimental discharge has not yet made the transition to enhanced confinement at this time. The E$\times$B shear was multiplied by 0.01 in the simulation of Fig. 3(b). A larger value produces a smaller amplitude jet and a value near one produces a transport barrier at larger radius without a jet. The computed growth rate in the region of the jet was about 0.03 c_s/a. This would have to be increased to 3.0 c_s/a in order to reconcile the jet solution with the standard quench rule. Such a large growth rate is not likely for ITG or TEM modes. Another possibility is that the predominantly trapped electron mode turbulence in this region does not follow the quench rule but is rather suppressed, but not totally turned off, by E$\times$B shear. A power law suppression factor [25,26] would allow the E$\times$B velocity shear to greatly exceed the linear growth rate without completely reducing the transport to neoclassical. A third possibility is that ETG modes produce some ion momentum transport which is not included in the model. This would allow the momentum diffusivity to decrease as the E$\times$B velocity shear increases well beyond the local ITG mode growth rate to the much larger ETG mode growth rate at short wavelenght. These are open questions related to the well known inconsistencies between the quench rule and experiment [3]. For example, quasilinear theory predicts that ion momentum and electron particle transport should become neoclassical if the ITG/TEM modes are quenched by E$\times$B shear. Experimentally, particle and ion toroidal momentum transport are often not reduced to neoclassical values within transport barrier regions with neoclassical ion thermal transport.

5. Summary

The drift-wave based transport models (Multi-Mode, GLF23) have been used to simulate the evolution of internal transport barriers in a number of discharges from several tokamaks. Three examples have been given in this paper. The models reproduce the onset and expansion of the internal transport barriers fairly accurately. The success of these models is a

confirmation of the ITG mode physics. In the models, ITG modes dominate the ion thermal and momentum transport prior to the formation of an internal transport barrier where E×B velocity shear quenches the ITG mode. The exact timing of the barrier formation and the threshold power or torque required are sensitive to the local plasma parameters. Attempts to simulate a discharge close to a transport barrier threshold can fail badly because the simulation ends up on the wrong side of the threshold. This makes it difficult to assess the statistical accuracy of the models for discharges with transport barriers. On the other hand, this same sensitivity makes the threshold a strong test of the theory of ITG suppression by E×B shear. There are still many unresolved issues concerning tokamak transport. The internal transport barriers provide a laboratory where non-ITG transport mechanisms can be studied. The transport due to ETG modes in the GLF23 model has not been guided by non-linear turbulence simulations and thus has a lower level of confidence than the ITG modeling. Non-linear simulations of the effect of E×B shear on trapped electron mode turbulence is also a high priority. The kinetic ballooning model in Multi-Mode is primitive. These modes could be included in the linear growth rate claculations by improving the electromagnetic parts of the models and extending the magnetic geometry to shaped equilibria. The current state of drift-wave based modeling of internal transport barriers is represented by the three examples given in this paper. The models are capable of reproducing interesting dynamical phenomena like step-wise barrier expansion and the poloidal spin-up precursor. These milestones indicate that the drift-wave theory of tokamak transport is on the right track.

Acknowledgments

References

[1]   WALTZ, R.E., *et al.*, Phys. Plasmas **2** (1995).
[2]   For a review see Burrell, K. H., Phys. Plasmas **4** (1997) 1499.
[3]   For a review see Staebler, G.M., Plasma Phys. and Control. Fusion, 40 (1997) 569.
[4]   BATEMAN, G., *et al.*, in Proceedings of the Sixteenth IAEA Fusion Energy Conference, (Montreal, Canada, 7-11, October) (IAEA, Vienna, 1996), Vol. II, 559-565.
[5]   BATEMAN, J.E., *et al.*, Phys. Plasmas **5** (1998) 1793.
[6]   BATEMAN, G., *et al.*, and SCOTT, B., Proceedings of the Seventeenth International Atomic Energy Agency Fusion Energy Conference, (Yokohama, Japan, 19–24 October, 1998) Vol. 4, 1569–1572.
[7]   NORDMAN, H., *et al.*, Nuclear Fusion **30** (1990) 983.
[8]   WEILAND, J. and HIROSE, A., Nuclear Fusion **32** (1992) 151.
[9]   NILSSON, J. and WEILAND, J., Nuclear Fusion **34** (1994) 803.
[10] WALTZ, R.E., STAEBLER, G.M., *et al.*, Phys. Plasmas **4** (1997) 2482.
[11] HAMMETT, G. and PERKINS, F., Phys. Rev. Lett. **64** (1990) 3019.
[12] DOMINGUEZ, R.R., and STAEBLER, G.M., Phys. Fluids, **B5** (1993) 3876.
[13] ZHU, P., *et al.*, Phys. Plasmas 7 (2000) 2898.
[14] KINSEY, J.E., STAEBLER, G.M., *et al.*, sumitted to Phys. Rev. Lett.
[15] BELL, R.E., *et al.*, Phys. Rev. Lett. **81** (1998) 1429.
[16] STAEBLER, G.M., KINSEY, J.E. in preparation.
[17] SINGER, C.E., *et al.*, Comput. Phys. Commun. **49** (1988) 275.
[18] The XPTOR code was written by J.E. Kinsey and G. M. Staebler making use of existing data handling packages written by R.E. Waltz, J. Konings and G. Batemen and a transport equation sovler written by G. Hammett. The code uses the MPI parallel library and is run on a Linux Beowulf cluster built by Jeff Candy.
[19] HINTON, F.L., KIM, Y.-B., Nuclear Fusion **34** (1994) 899.
[20] TAYLOR, J.B., CONNOR, J.W., and HELANDER, P., Phys. Plasmas **5**, 3065 (1998).
[21] ZHU, P., HORTON, W., and SUGAMA, H., Phys. Plasmas, **6** (1999) 2503.
[22] HAMAGUCHI, S. and HORTON, W., Phys. Fluids B, **4** (1992) 319.
[23] STAEBLER, G.M., Phys. Rev. Lett. **84** (2000) 3610.
[24] TSANG, K.T. and FRIEMAN, E.A., Phys. Fluids 19 (1976) 747.
[25] SHAING, K.C., *et al.*, in Proc. 12th Int. Conf.on Plasma Phys. and Control. Fusion Res., Nice 1988 (IAEA, Vienna, 1989) Vol.II, pp.13.
[26] BIGLARI, H., DIAMOND, P.H. and TERRY, P.W., Phys. Fluids, **B2** (1990) 1.